

# Exotic Dirac Cones on the Band Structure of $\alpha$ -STF<sub>2</sub>I<sub>3</sub> at Ambient Temperature and Pressure

Toshio NAITO<sup>1</sup>\*, Ryusei Doi<sup>1</sup>, and Yoshikazu SUZUMURA<sup>2</sup>

<sup>1</sup>*Department of Chemistry, Ehime University, Matsuyama 790-8577, Japan*

<sup>2</sup>*Department of Physics, Nagoya University, Nagoya 464-8602, Japan*

The quasi-two-dimensional molecular semimetallic conductor  $\alpha$ -STF<sub>2</sub>I<sub>3</sub> is isostructural with  $\alpha$ -ET<sub>2</sub>I<sub>3</sub>. The latter possesses a unique band structure showing a zero-gap state with Dirac cones under high pressure, whereas the band structure of the former has been elusive because of heavy disorder at all the donor sites. To elucidate the band structure of  $\alpha$ -STF<sub>2</sub>I<sub>3</sub>, a theoretical method based on the observed atomic parameters at 296 K and 1 bar has been proposed. The results suggest that the STF salt should have a band structure with Dirac cones under ambient pressure and temperature, which should promote future experimental studies on this system. Using the extended Hückel method, we demonstrate that the Dirac points of  $\alpha$ -STF<sub>2</sub>I<sub>3</sub> are aligned to be symmetric with respect to a time reversal invariant momentum (TRIM). Such novel Dirac cones, where the energy difference between the conduction and valence bands has considerable anisotropy, are clarified in terms of the parity of the wavefunction at the TRIM. We propose the conductivity measurement on the present  $\alpha$ -STF<sub>2</sub>I<sub>3</sub>, which is expected to show a large anisotropy as a characteristic of the present Dirac electrons.

In a recent development in organic conductors,<sup>1,2)</sup> Dirac electrons have been studied extensively since the zero-gap state with Dirac cones<sup>3)</sup> has been found in  $\alpha$ -ET<sub>2</sub>I<sub>3</sub> (ET = BEDT-TTF = bis(ethylenedithio)tetrathiafulvalene) under high pressure (>1.5 GPa) using a tight-binding model with transfer integrals.<sup>2,4-7)</sup>  $\alpha$ -ET<sub>2</sub>I<sub>3</sub> is isostructural with  $\alpha$ -BETS<sub>2</sub>I<sub>3</sub><sup>8)</sup> and  $\alpha$ -STF<sub>2</sub>I<sub>3</sub> as the  $\alpha$  salt,<sup>9-12)</sup> (BETS = BEDT-TSF = bis(ethylenedithio)tetraselenafulvalene). They share a three-quarter-filled band and four molecules per unit cell. The organic donor STF,<sup>9-12)</sup> where STF is bis(ethylenedithio)diselenadithiafulvalene, is an analogue of ET and BETS, has produced a number of salts isostructural with those of ET and BETS, including  $\alpha$ -D<sub>2</sub>I<sub>3</sub> (D = ET, STF, and BETS) (Fig. 1).

The most important difference between STF and the other organic donors (ET and BETS) lies in the molecular symmetry. Because of the lower symmetry, all the known STF salts include orientational disorder at the donor sites in the crystals. However, regarding electrical, magnetic, and optical properties in the solid states, many of the STF salts exhibit intermediate behavior between the isostructural ET and BETS salts, as if the solids do not contain any disorder but consist of a symmetrical donor containing imaginary atoms between selenium and sulfur at the inner chalcogen atoms.<sup>9-12)</sup> The observation suggests that STF salts should lie between the isostructural ET and BETS salts with stronger/weaker intermolecular interactions among donor molecules than the ET/BETS salts. A typical example is  $\alpha$ -D<sub>2</sub>I<sub>3</sub> (D = ET, STF, BETS), where one can recognize systematic variation in the electrical behavior in the three salts as shown in Fig. 1.<sup>10)</sup>

For  $\alpha$ -BETS<sub>2</sub>I<sub>3</sub>, the temperature dependence of the

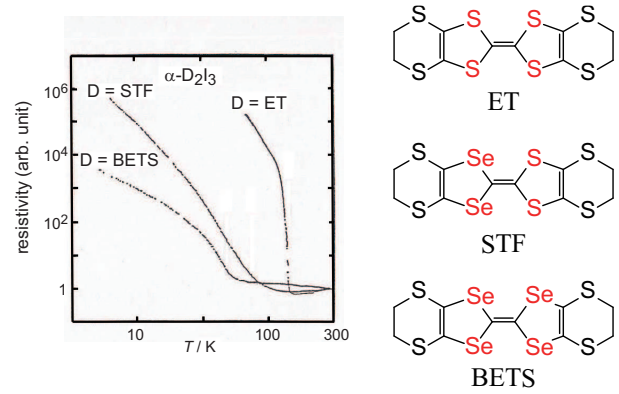


Fig. 1. (Color online) Electrical behavior of  $\alpha$ -D<sub>2</sub>I<sub>3</sub><sup>10)</sup> (D = ET, STF, and BETS) with the molecular structures of donor D.

spin susceptibility<sup>13,14)</sup> shows a marked decrease even in the normal state, suggesting an unusual electronic state ascribed to the peculiar energy band. The band calculation indicates that there should be a Dirac point with overtilted cones, and that  $\alpha$ -BETS<sub>2</sub>I<sub>3</sub> should remain metallic.<sup>15)</sup> The zero-gap state is studied by adding a site potential<sup>15)</sup> or taking account of the correlation,<sup>16)</sup> where the latter shows the Dirac point near the insulating state followed by the merging of Dirac points at one of the time reversal invariant momenta (TRIMs). In this context, the mechanism to produce Dirac points should be more complicated in  $\alpha$ -BETS<sub>2</sub>I<sub>3</sub> than in  $\alpha$ -ET<sub>2</sub>I<sub>3</sub>, although a Dirac point by itself originates from the intrinsic property of band crossing. Although  $\alpha$ -STF<sub>2</sub>I<sub>3</sub> is also expected to show such an electronic state owing to the close similarities in the molecular structures, the band structure is yet to be clarified.

In this Letter, we demonstrate the zero-gap state with

\*E-mail: tnaito@ehime-u.ac.jp

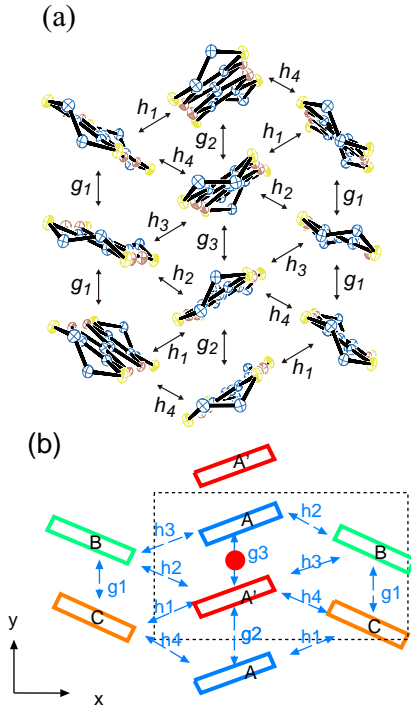


Fig. 2. (Color online) Molecular arrangement of STF in  $\alpha$ -STF<sub>2</sub>I<sub>3</sub>. (a) Intermolecular interactions in the conduction sheet. Brown spheres indicate disordered chalcogen atoms (Se or S), which are included in every STF molecule. Arrows indicated by  $g_i$  ( $i = 1-3$ ) and  $h_j$  ( $j = 1-4$ ) show intermolecular interactions. Hydrogen atoms are omitted for clarity. (b) Schematic picture of (a). A, B, and C indicate crystallographically independent STF molecules, while A and A' are interrelated by an inversion center (closed circle). Four molecules in the same unit cell (dotted line) have a common phase of wavefunctions.

the Dirac cone in  $\alpha$ -STF<sub>2</sub>I<sub>3</sub> by a modified method of estimation of transfer integrals, which is based on single-crystal X-ray structural analysis [Fig. 2(a)].<sup>10</sup> The paper is organized as follows. First, we propose a tentative new method for  $\alpha$ -STF<sub>2</sub>I<sub>3</sub> to obtain the transfer integrals for the tight-binding model. Next, on the basis of this model, we show theoretically the zero-gap state with Dirac cones, where the Dirac points are aligned toward a TRIM.

In the band calculation of  $\alpha$ -STF<sub>2</sub>I<sub>3</sub>, the most difficult problem is to satisfy the crystallographic requirements in symmetries, which could not be done by locating unsymmetrical donor wavefunctions at the STF sites. To calculate the band structure, it is crucial to retain the crystallographic symmetries required for both a particular donor site and the entire donor arrangement.

In this study, we have noticed that all the occupancies at the inner chalcogen atoms are 50:50 = S:Se in the STF salt (Tables S1 and S2 in Ref. 17). Thus, we carried out a band structure calculation, assuming that the effective transfer integrals ( $t_{\text{eff}}$ ) between disordered STF molecules should be treated approximately using the averaged values of all the possible orientations, i.e., four patterns of molecular arrangements in each pair of interacting STF molecules (Fig. 3). The grounds for this assumption are obtained from the single-crystal X-ray

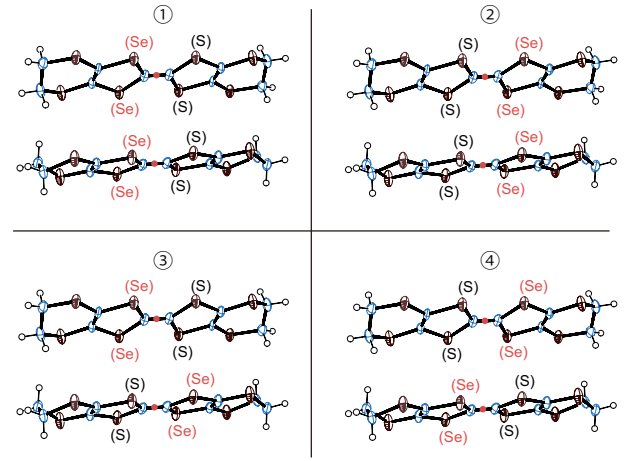


Fig. 3. (Color online) Four patterns of possible arrangements of an interacting pair of STF molecules considered in the calculation, where ①, ②, ③, and ④ correspond to those in Table S4 in Ref. 17. All these patterns occur in the crystal with an equal probability to each other to reproduce the observed structure.

structural analysis on  $\alpha$ -STF<sub>2</sub>I<sub>3</sub><sup>17</sup> [Fig. 2(a)].<sup>10</sup> The asymmetric unit contains two STF molecules in total: an entire STF at a general position plus two halves of STF on the inversion centers, all of which are disordered in the molecular orientation (Fig. 3). The occupancies of S/Se in the inner chalcogen atoms of STF are all 50%/50%. This means that the electron densities of the inner four chalcogen atoms in every STF molecule are averaged to satisfy the inversion symmetry. The obtained transfer integrals corresponding to  $g_1, g_2, g_3, h_1, h_2, h_3$ , and  $h_4$  in Figs. 2(a) and 2(b) are summarized in Table S4 (Model A) in Ref. 17 based on the Hückel parameters in Table S3 in Ref. 17. We also examined the parameter dependence of the results, and have confirmed that a different set of atomic parameters obtained from independent structural analysis also gave qualitatively the same results: a band structure with Dirac cones [Tables S2 and S4 (Model B), and Figs. S1(a) – S1(c)].<sup>17</sup> As shown in Figs. 4, 5(a), and 5(b), the calculation suggested that  $\alpha$ -STF<sub>2</sub>I<sub>3</sub> should have a band structure characterized by its Dirac cones at 296 K and 1 bar. The tight-binding band structure obtained on the basis of these transfer integrals qualitatively accounts for the electrical and magnetic properties of  $\alpha$ -STF<sub>2</sub>I<sub>3</sub>, which should also be further examined experimentally.

Here, we make a brief comment on the effect of disorder on the band structure and electronic properties. The disorder should affect the intrinsic electronic properties of Dirac cones and those of a zero-gap semiconductor in  $\alpha$ -STF<sub>2</sub>I<sub>3</sub>, which limits ourselves to comparing the calculated band structure with experimental results. Thus, it is important to estimate the energy scale of disorder effects to clarify the energy and temperature ranges where the band structure will be directly manifested in the electronic properties. In Fig. 1,  $\alpha$ -STF<sub>2</sub>I<sub>3</sub> exhibits nearly temperature-independent electrical behavior at  $T \geq 100$  K, which is the behavior characteristic to a zero-gap semiconductor having Dirac cones. Below  $\sim 100$

K, the resistivity increases with decreasing temperature. Thus, our calculation results can be compared with the observed resistivity behavior at  $T \geq 100$  K, and the disorder effect should overwhelm the intrinsic behavior below  $\sim 100$  K.

Now, we examine theoretically such an exotic band structure in  $\alpha$ -STF<sub>2</sub>I<sub>3</sub> with inversion symmetry between A and A', which is crucial for the existence of the Dirac point.<sup>18)</sup> This mechanism is analyzed in terms of the parity inversion properties of energy bands at the TRIM ( $\mathbf{G}/2$  with  $\mathbf{G}$  being a reciprocal lattice vector).<sup>19)</sup>

From Ref. 17, the transfer energies (Model A) for a tight-binding model with a square lattice are obtained as  $g_1 = 0.0015$ ,  $g_2 = 0.1420$ ,  $g_3 = 0.0450$ ,  $h_1 = -0.2767$ ,  $h_2 = -0.2847$ ,  $h_3 = 0.0092$ , and  $h_4 = 0.0057$ , in the unit of eV [Fig. 2(b)]. The Hamiltonian is expressed as

$$H = \sum_{i,j=1}^N \sum_{\alpha,\beta=1}^4 t_{i,j;\alpha,\beta} a_{i,\alpha}^\dagger a_{j,\beta}, \quad (1)$$

where  $a_{i,\alpha}^\dagger$  denotes a creation operator of an electron of molecule  $\alpha$  [A(1), A'(2), B(3), and C(4)] in the unit cell at the  $i$ th lattice site. The transfer energies,  $g_1, \dots, h_4$  are given by  $t_{i,j;\alpha,\beta}$ . By using the Fourier transform  $a_j = 1/N^{1/2} \sum_{\mathbf{k}} a_{\mathbf{k}}(\mathbf{k}) \exp[i\mathbf{k} \cdot \mathbf{r}_j]$ , Eq. (1) is rewritten as

$$\begin{aligned} H &= \sum_{\mathbf{k}} \sum_{\alpha,\beta=1}^4 t_{\alpha,\beta}(\mathbf{k}) a_{\alpha}^\dagger(\mathbf{k}) a_{\beta}(\mathbf{k}) \\ &= \sum_{\mathbf{k}} \sum_{n=1}^4 E_n(\mathbf{k}) b_n(\mathbf{k})^\dagger b_n(\mathbf{k}), \end{aligned} \quad (2)$$

where  $\mathbf{k} = (k_x, k_y)$  and the lattice constant is taken as unity. The matrix elements  $t_{\alpha,\beta}(\mathbf{k})$  ( $\alpha, \beta = 1, \dots, 4$ ) are given by  $t_{12}(\mathbf{k}) = g_3 + g_2 Y$ ,  $t_{13}(\mathbf{k}) = h_3 + h_2 \bar{X}$ ,  $t_{14}(\mathbf{k}) = h_4 Y + h_1 \bar{X} Y$ ,  $t_{23}(\mathbf{k}) = h_2 + h_3 \bar{X}$ ,  $t_{24}(\mathbf{k}) = h_1 + h_4 \bar{X}$ ,  $t_{34}(\mathbf{k}) = g_1 + g_1 \bar{Y}$ , and  $t_{ij}(\mathbf{k}) = t_{ji}^*(\mathbf{k})$ ,  $t_{ii}(\mathbf{k}) = 0$ , where  $X = \exp[ik_x] = \bar{X}^*$  and  $Y = \exp[ik_y] = \bar{Y}^*$ , and the choice of the phase is the same as that of Ref. 3. The eigenvalue, i.e., the energy  $E_n(\mathbf{k})$  [ $E_1(\mathbf{k}) > E_2(\mathbf{k}) > E_3(\mathbf{k}) > E_4(\mathbf{k})$ ] is calculated by diagonalizing the  $4 \times 4$  matrix Hamiltonian, where  $b_n$  denotes an operator corresponding to  $E_n(\mathbf{k})$ .

Figure 4 shows  $E_1(\mathbf{k})$  and  $E_2(\mathbf{k})$  on the plane of the 1st Brillouin zone. There are two Dirac points with  $E_1(\mathbf{k}_D) = E_2(\mathbf{k}_D) = \varepsilon_D$ , which are given by  $\mathbf{k}_D/\pi - (0, 1) = (k_x/\pi, k_y/\pi - 1) = \pm(0.61, -0.18)$ . Hereafter, we take the chemical potential ( $= 0.3995$  eV in the original Hamiltonian) as the origin of the energy, which coincides with  $\varepsilon_D$  due to the 3/4-filled band. A pair of Dirac points are symmetric with respect to the Y ( $= 0, \pi$ ) point. The difference between  $E_1(Y)(> 0)$  and  $E_2(Y)(< 0)$  is smaller than those of the other TRIMs. In fact, their energies of [ $E_1(\mathbf{G}/2)$ ,  $E_2(\mathbf{G}/2)$ ] are obtained as (0.2484, -0.4037), (0.0916, -0.2137), (0.0340, -0.0566), and (0.0663, -0.0468) for  $\Gamma = (0, 0)$ , X ( $= \pi, 0$ ), Y ( $= 0, \pi$ ), and M ( $= \pi, \pi$ ), respectively. The zero-gap state is obtained because  $E_1(\mathbf{k}) \geq \varepsilon_D \geq E_2(\mathbf{k})$ .

Figure 5(a) shows a contour plot of the energy difference  $\Delta = E_1(\mathbf{k}) - E_2(\mathbf{k})$ , where the Dirac point man-

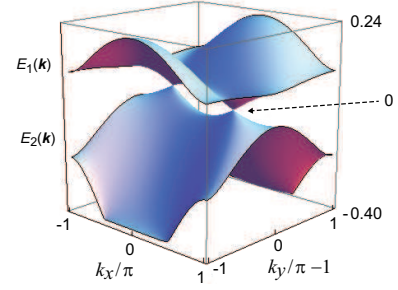


Fig. 4. (Color online) Energy bands of  $E_1(\mathbf{k})$  and  $E_2(\mathbf{k})$  as functions of  $\mathbf{k}$ . The Dirac points exist at  $\mathbf{k}_D = (k_x/\pi, k_y/\pi - 1) = \pm(0.61, -0.18)$ . The relation  $E_1(\mathbf{k}) \geq E_1(\mathbf{k}_D) = E_2(\mathbf{k}_D) \geq E_2(\mathbf{k})$  suggests the zero-gap state. The energy at the Dirac point is equal to the chemical potential.

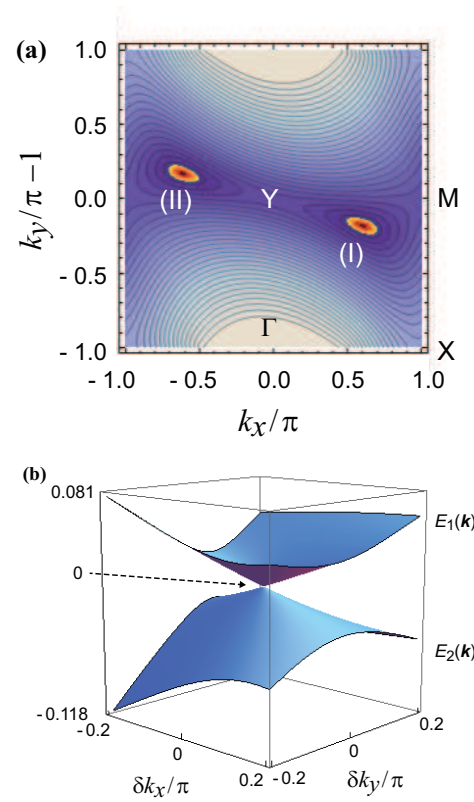


Fig. 5. (Color online) (a) Contour plot of  $E_1(\mathbf{k}) - E_2(\mathbf{k})$ . The orange region denotes  $0 < E_1(\mathbf{k}) - E_2(\mathbf{k}) < 0.03$ , where the Dirac points with  $\mathbf{k}_D/\pi - (0, 1) = (k_x/\pi, k_y/\pi - 1) = (0.61, -0.18)$  (I), and  $(-0.61, 0.18)$  (II) are seen at the center of each orange region. (b) Dirac cones for the Dirac point (I) in (a) on the plane of  $-0.2 < \delta k_x/\pi < 0.2$  and  $-0.2 < \delta k_y/\pi < 0.2$ .  $\delta \mathbf{k} = \mathbf{k} - \mathbf{k}_D$ .  $\mathbf{k}_D/\pi - (0, 1) = (0.61, -0.18)$ .

ifests itself at the center of the orange (bright) region ( $0 < \Delta < 0.03$ ). Two Dirac points  $\mathbf{k}_D$  shown by (I) and (II) are symmetric with respect to the Y point. The orange region is elongated toward the Y-point. The contour for the fixed (small)  $\Delta$  shows an ellipse, where the ratio of major and minor axes is about 2.4.

Figure 5(b) shows the band energy with Dirac cones

Table I. Parity eigenvalue  $E_P(j, \mathbf{G}/2) (= \pm 1)$  for eigenfunction  $E_j(\mathbf{G}/2)$

	$\Gamma$	X	Y	M
$E_1$	1	-1	-1	-1
$E_2$	1	1	1	1
$E_3$	-1	-1	-1	-1
$E_4$	1	-1	1	1

around the Dirac point (I), where the linear dispersion is verified. In terms of the velocities  $v_x$  and  $v_y$  ( $v_x > v_y$ ) corresponding to the minor and major axes of the ellipse, respectively, the band energy  $E_j$  ( $j = 1, 2$ ) for the conduction and valence bands may be written as

$$E_j(\mathbf{q}) = v_t q_t - (-1)^j \sqrt{(v_x q_x)^2 + (v_y q_y)^2}, \quad (3)$$

where  $\mathbf{q} = \mathbf{k} - \mathbf{k}_D$ . The quantity  $q_x(q_y)$  denotes the momentum for the minor (major) axis of Fig. 5(a), where  $q_y$  is parallel to the elongated one. The quantities  $v_t$  and  $q_t$  denote the velocity and momentum for the tilt of the cone, respectively, where the tilt occurs almost along the  $q_x$  direction and  $v_t/v_x \sim 0.2$  is much smaller than that of  $\alpha\text{-ET}_2\text{I}_3$ .<sup>2)</sup> From Fig. 5(a) and the contour of  $E_j(\mathbf{k})$ , ( $j = 1, 2$ ), it is found that the Dirac cone with a linear dispersion may be valid for  $E_1(\mathbf{k}) - E_2(\mathbf{k}) < 0.05$ .

Now, we examine the presence of Dirac points by calculating the parity of the eigenfunction at the TRIMs as shown in Fig. 5(a). The parity is calculated using the inversion matrix,<sup>19)</sup> which is a  $\pi$ -rotation around the inversion center of the midpoint of A and A' [closed circle in Fig. 2(b)]. The  $4 \times 4$  inversion matrix  $\hat{P}_i$  has only the diagonal elements given by 1, -1,  $e^{-ik_x}$  and  $e^{-ik_x - ik_y}$ . Using  $[\hat{H}(\mathbf{G}/2), \hat{P}_i(\mathbf{G}/2)] = 0$  and the transformation of the base<sup>20)</sup> [ $u_1 = 2^{-1/2}(u_A + u_{A'})$  and  $u_2 = -i2^{-1/2}(u_A - u_{A'})$ ], we obtain  $\hat{P}_i(\mathbf{G}/2)\Psi_j(\mathbf{G}/2) = E_P(j, \mathbf{G}/2)\Psi_j(\mathbf{G}/2)$ , where  $E_P(j, \mathbf{G}/2) = \pm 1$  denotes the parity eigenvalue, and  $\Psi_j(\mathbf{G}/2)$  is the eigenfunction for  $E_j(\mathbf{G}/2)$ . This parity for  $\alpha\text{-STF}_2\text{I}_3$  is summarized in Table I, which satisfies the condition for the existence of the Dirac points,<sup>19, 21)</sup>

$$P = E_P(1, \Gamma)E_P(1, X)E_P(1, Y)E_P(1, M) = -1. \quad (4)$$

Note that Eq. (4) becomes +1 when the insulating state is expected, i.e., the absence of Dirac points after merging by the level crossing between  $E_1$  and  $E_2$ .

We also discuss the relevance of the calculated band structure to the experiment on the conductivity of  $\alpha\text{-STF}_2\text{I}_3$ , which suggests the zero-gap behavior under ambient pressure. The experimental finding of the maximum conductivity in addition to the anisotropy of the cone being larger than that of  $\alpha\text{-ET}_2\text{I}_3$ <sup>22)</sup> is of interest to justify the present Dirac cone. Our calculation shows that  $\sigma_x/\sigma_y \simeq (v_x/v_y)^2 \simeq 5$ ,<sup>23)</sup> whereas the direction of the maximum conductivity is sensitive to the choice of transfer energies, and the comparison with the experiment remains as a future problem.

In addition to Eq. (1), we briefly mention the effect of the local potentials  $V_B$  and  $V_C$  on the B and C sites,

which has been examined for  $\alpha\text{-ET}_2\text{I}_3$  in Ref. 15. The present calculation for  $|V_B| < 0.2$ ,  $|V_C| < 0$  shows that the zero-gap state exists in region (I)  $V_B \leq 0$  and  $V_C \leq 0$  and that the boundary followed by merging between the zero-gap state and the insulating state is located slightly outside of region (I), whereas the metallic region as found in Ref. 15 is absent owing to the lack of overtilted Dirac cones.

In summary, we have reported on the following two subjects. (1) We have evaluated the transfer integrals of  $\alpha\text{-STF}_2\text{I}_3$  for the tight-binding model based on our proposal of approximation treating the disorder at the STF sites. (2) Analyzing the model in terms of parity at the TRIMs, we found the zero-gap state with Dirac cones. Such Dirac cones obtained from (1) and (2) could be justified by the measurement of anisotropic conductivity, which belongs to the most fundamental and practical experiments.

### Acknowledgements

The authors acknowledge helpful discussion with Naoya Tajima at Toho University.

- 1) For review: H. Seo, C. Hotta, and H. Fukuyama, Chem. Rev. **104**, 5005 (2004).
- 2) K. Kajita, Y. Nishio, N. Tajima, Y. Suzumura, and A. Kobayashi, J. Phys. Soc. Jpn. **83**, 072002 (2014).
- 3) S. Katayama, A. Kobayashi, and Y. Suzumura, J. Phys. Soc. Jpn. **75**, 054705 (2006).
- 4) R. Kondo, S. Kagoshima, and J. Harada: Rev. Sci. Instrum. **76** (2005) 093902.
- 5) Y. Suzumura and A. Kobayashi, Crystals **2**, 266 (2012).
- 6) N. Tajima, Y. Nishio, and K. Kajita, Crystals **2**, 643 (2012).
- 7) N. Tajima, Crystals **8**, 126 (2018).
- 8) R. Kato, H. Kobayashi, and A. Kobayashi, Synth. Met. **41–43**, 2093 (1991).
- 9) T. Naito, A. Miyamoto, H. Kobayashi, R. Kato, and A. Kobayashi, Chem. Lett. **21**, 119 (1992).
- 10) T. Naito, Dr. Thesis, Graduate School of Science, The University of Tokyo, Tokyo (1995). <http://dl.ndl.go.jp/info:ndljp/pid/3127801>.
- 11) M. Inokuchi, H. Tajima, A. Kobayashi, T. Ohta, H. Kuroda, R. Kato, T. Naito, and H. Kobayashi, Bull. Chem. Soc. Jpn. **68**, 547 (1995).
- 12) T. Naito, H. Kobayashi, and A. Kobayashi, Bull. Chem. Soc. Jpn. **70**, 107 (1997).
- 13) Y. Takano, K. Hiraki, Y. Takada, H. M. Yamamoto, and T. Takahashi, J. Phys. Soc. Jpn. **79**, 104704 (2010).
- 14) K. Hiraki, S. Harada, K. Arai, Y. Takano, T. Takahashi, N. Tajima, R. Kato, and T. Naito, J. Phys. Soc. Jpn. **80**, 014715 (2011).
- 15) K. Kondo, S. Kagoshima, N. Tajima, and R. Kato, J. Phys. Soc. Jpn. **78**, 114714 (2009).
- 16) T. Morinari and Y. Suzumura, J. Phys. Soc. Jpn. **83**, 094701 (2014).
- 17) Supplemental materials of the present paper. Tables of atomic coordinates, the parameters used in the calculation of transfer energies, the calculated transfer energies, and the figure of the band structures of  $\alpha\text{-STF}_2\text{I}_3$  are provided online.
- 18) Y. Suzumura, J. Phys. Soc. Jpn. **85**, 053708 (2016).
- 19) F. Piéchon and Y. Suzumura, J. Phys. Soc. Jpn. **82**, 03703 (2013).
- 20) F. Piéchon and Y. Suzumura, J. Phys. Soc. Jpn. **82**, 123703 (2013).
- 21) L. Fu and C. L. Kane, Phys. Rev. B **76**, 045302 (2007).
- 22) N. Tajima, private communication.

---

23) Y. Suzumura, I. Proskurin, and M. Ogata, J. Phys. Soc. Jpn. **83**, 023701 (2014).